Supporting Information

Light-On and Power-On: A Dual Mode Active De-/Anti-Icing System Using Liquid Metal-Based Photothermal and Electrothermal Pastes

Chimin Song,[1] Soonchul Kwon,[2] Jungmin Lee,[3] Yongmin Cho,[1] Joohyung Lee[1,]*

[1]Department of Chemical Engineering, Myongji University, 116 Myongji-ro, Cheoin-gu, Yongin, Gyeonggi-do, 17058, Korea

[2]Department of Civil and Environmental Engineering, Pusan National University, 2 Busandaehak-ro 63beon-gil, Geumjeong-gu, Busan, 46241, Korea

[3]Land & Housing Institute, Korea Land & Housing Corporation, 462-2 Jeonmin-dong, Useong-gu, Daejeon, 305-731, Korea

[*]Corresponding author (email: ljbro@mju.ac.kr)

Experimental Details

Materials. LM Ga and EGaIn were purchased from Gallant Metals (USA) and Suzhou Haichuan Rare Metal Products (China), respectively. Alumina microplates (maximum Feret basal-plane diameter: 4.09 ± 1.73 μm; thickness: 1.18 ± 0.25 μm) were obtained from PACE Technologies (USA). Silicon (Si) powder and sodium dodecyl sulfate (SDS) were purchased from Daejung Chemicals & Metals (Korea). *n*-Eicosane was obtained from Alfa Aesar (USA). Bisphenol A diglycidyl ether (BADGE), hexahydro-4-methylphthalic anhydride (HMPA), and 2-ethyl-4-methylimidazole (EMI) were purchased from Sigma-Aldrich (USA). Paraffin oil and hexane were purchased from Samchun Chemicals (Korea) and Duksan Pure Chemicals (Korea), respectively. Deionized (DI) water with a resistivity of 18.2 MΩ·cm (Direct-Q® Water Purification System) was used throughout the experiments.

Preparation of Ga fillers. Ga microdroplets were prepared by sonicating 5 g of bulk Ga in 20 mL of paraffin oil using an HD 4200 ultrasonic homogenizer (Bandelin, Germany) for 20 min at an amplitude of 115 μm, employing a pulsed mode of 3 s on / 2 s off. After sonication, the resulting dispersion was washed with excess hexane via centrifugation (800 rpm, 10 min) to remove the paraffin oil. This washing process was repeated five times. The collected Ga microdroplets were subsequently dried in an oven at 100 °C for 24 hours, yielding the final product.

Preparation of PCM fillers. PCM microparticles were prepared by dispersing 2 g of bulk *n*-eicosane into 10.1 mL of an aqueous surfactant solution containing SDS (0.01 wt.%) at 100 °C, using a HG-15A rotor–stator homogenizer (Daihan Scientific, Korea) operated at 10800 rpm for 10 min. The application temperature of 100 °C was selected primarily to ensure the complete melting of bulk *n*-eicosane prior to emulsification. Although the melting point of *n*-

eicosane is around 37 °C, operating at a significantly higher temperature reduces the viscosity of both the oil and aqueous phases, thereby facilitating efficient droplet breakup during high-shear homogenization. In addition, the elevated temperature helps mitigate excessive foaming induced by SDS during homogenization by lowering the viscosity of the continuous phase and promoting faster bubble collapse. The resulting emulsion was frozen at -83–86 °C for 24 hours, and subsequently vacuum-dried for 72 hours to remove water, yielding PCM microparticles in powder form.

Preparation of PCM@Ga hybrid fillers. PCM@Ga hybrid fillers were prepared by adding 6.54 g of the previously prepared PCM microparticles to 1.46 g of bulk Ga, followed by mixing with an HPM-1.5H planetary mixer (Han Tech, Korea) at 800 rpm for 3 min. The mixing was repeated twice. The resulting mixture was obtained in powder form, and no additional washing or drying processes were required.

Preparation of photothermal system. Photothermal pastes were prepared by dispersing fillers (alumina and either PCM@Ga or Ga) into a 3 mL epoxy mixture composed of equimolar amounts of BADGE and HMPA, along with 0.03 g of EMI as a curing accelerator. The mixture was homogenized at room temperature (25 °C) using a BL620D overhead stirrer (Misung Scientific, Korea) at 800 rpm for 2 min, yielding a paste-type photothermal system. Alumina, used as a co-filler with the photothermal agents, was added to the epoxy matrix to enhance the mechanical properties of the resulting composites. In addition, the suspended alumina effectively suppressed the sedimentation of the photothermal agents during the thermal curing process. For PCM@Ga-containing formulations, the total filler volume fraction (ϕ_F) was fixed at 0.5, while the individual volume fractions of alumina (ϕ_A) and PCM@Ga ($\phi_{PCM@Ga}$) were varied among 0.1, 0.2, 0.3, and 0.4. As a control, Ga-containing photothermal systems were

prepared with the same alumina content and an equivalent volume of Ga, calculated based on the Ga content in the corresponding PCM@Ga formulations. As an additional control, ARE matrices without photothermal agents were prepared by mixing only alumina into the epoxy matrix under the same conditions, at $\phi_F = \phi_A = 0.5$. For thermal curing, the uncured photothermal pastes were cast into molds with either a disk shape (3.5 cm in diameter) or a rounded-square shape (6.7 cm × 6.7 cm) with a thickness of 5 mm. The cast pastes were then thermally cured in a muffle furnace at 150 °C for 2 hours, yielding the final solid-state photothermal specimens.

Electrothermal system. Electrothermal pastes were prepared by incorporating Si powder into bulk EGaIn at volume fractions (ϕ_{Si}) of 0.1, 0.2, and 0.3. The mixtures were homogenized using a PULVERISETTE 6 planetary mixer (Fritsch, Germany) at 500 rpm for 120 min, yielding paste-type electrothermal systems. The prepared pastes were screen-printed onto pre-cured ARE matrix substrates using a customized stencil mask made of adhesive tape (three stacked layers, total thickness: 1.8 mm), thereby forming patterned Joule-heating structures. For all patterns, the printed lines had a uniform length and width of 5 cm and 0.2 cm, respectively. The spacing between adjacent lines was set to 2.2 cm for the Line 3 pattern, 1 cm for the Line 5 pattern, 0.6 cm for the Line 7 pattern, and 0.4 cm for the Line 9 pattern.

Integrated System. An integrated system was fabricated by sequentially depositing both electrothermal and photothermal components onto a pre-cured ARE matrix substrate with a rounded-square shape (6.7 cm × 6.7 cm). First, an electrothermal paste ($\phi_{Si} = 0.3$) was screen-printed in the Line 7 pattern onto the substrate. Subsequently, a photothermal paste ($\phi_F = \phi_A + \phi_{PCM@Ga} = 0.2 + 0.3 = 0.5$) was applied as a 5 mm-thick layer over the printed pattern. The coated mass per unit substrate area is approximately 1.13 g/cm². The assembly was then

thermally cured at 150 °C for 2 hours, completing the fabrication of the integrated system.

Heating Performance Evaluation. The heating performance of the photothermal, electrothermal, and integrated systems was evaluated under either ambient conditions (25 °C) or cold conditions (–20 °C) inside a commercial freezer (C15, Alpicool, China). Photothermal experiments were performed using a Class AAA solar simulator (SciSun-300, Sciencetech Inc., Canada) equipped with a 300 W xenon short-arc lamp and a Class A AM 1.5G optical filter, compliant with the ASTM E927-19 and IEC 60904-9 standards. The simulator provides a spectral output closely matching the AM 1.5G reference spectrum, with a spectral mismatch of $< \pm 25$ % across 400–1100 nm. The irradiance at the sample plane was calibrated to 1 SUN (0.1 W/cm²) using a certified silicon reference cell (Sciencetech SSIVT-REF), with the lamp-to-sample distance appropriately adjusted. The illuminated area (≈50 × 50 mm²) exhibited Class A uniformity (≤ 1.3 %). Samples were positioned horizontally under normal incidence (0°), irradiated with varying intensities (0.5, 0.75, and 1 SUN) in still ambient air (25 ± 1 °C) without forced convection, and the temperature evolution was recorded over time. For electrothermal heating evaluation, an IT6720 power supply (ITECH Electronics, Korea) was used to apply various voltages (1, 1.5, 2, 3, and 4 V) to the screen-printed electrothermal patterns, and the resulting temperature changes were recorded over time. For dual-mode operation, both simulated sunlight and electrical power were simultaneously applied, and the temperature profiles were similarly recorded to assess the combined heating performance. For temperature monitoring, infrared (IR) thermography was conducted using an Xi 400 infrared camera (Optris Infrared Sensing, USA) with a fixed emissivity setting of 0.95, following the standard practice commonly adopted for polymeric, painted, oxidized, and other nonmetallic surfaces (typical emissivity≈0.90–0.98). For the EGaIn-based electrothermal patterns, a thin polyethylene (PE)

film (thickness: 100 μm) was placed over the printed pattern to provide a uniform, high-emissivity surface. The IR camera recorded the temperature of the PE surface to monitor the relative heating behavior as a function of applied voltage and pattern geometry. In the photothermal composites, micronized Ga@PCM particles appeared dark and, once embedded within the epoxy matrix, exhibited optically diffuse surfaces without noticeable reflectivity, thereby eliminating emissivity-related uncertainties. In the integrated system, where the electrothermal layer was covered by the photothermal coating, all IR images correspond to the outer photothermal surface, whose emissivity closely approximates that of the polymer matrix. To ensure measurement reliability, contact-type thermocouple readings were acquired simultaneously at representative surface locations; the measured values agreed with the IR data within ±0.53 °C, confirming the validity of the reported temperature changes.

De-icing and Anti-icing Tests. For de-icing tests, cubic ice blocks (2.5 cm × 2.5 cm × 2.5 cm) were prepared using a commercial mold in a freezer set to −83 to –86 °C. The ice cubes were placed at the center of the integrated photo-/electrothermal system surface under cold environmental conditions (-20 °C) and subjected to photothermal, electrothermal, or dual-mode heating. The dynamic morphological changes of the ice were monitored over time for each heating mode. Additionally, fine frost generated in the −83 to –86 °C freezer was collected and uniformly deposited to fully over the system surface. De-icing tests under different heating modes were then conducted under the same conditions. For anti-icing tests, water droplets of equal volume (400 μL) were placed on the surface of the integrated system and carefully observed to determine whether freezing occurred over time under each heating mode.

Morphological characterization. The morphologies of PCM and PCM@Ga particles were examined using an BX51 optical microscope (Olympus, Japan) and an EM-30AX scanning

electron microscope (COXEM, Korea) equipped with energy-dispersive spectroscopy. The internal microstructures of the electrothermal systems were also investigated using the same SEM/EDS setup.

Rheological characterization. Rheological properties of the photothermal and electrothermal pastes were measured using a HAAKE MARS-40 rheometer (Thermo Fisher Scientific, USA) equipped with parallel plates (diameter: 35 mm). Oscillatory measurements were conducted under a constant shear stress of 10 Pa over a frequency range of 0.01 to 100 s^{-1} to determine G′, G″, and η* of the samples. The gap distance was experimentally optimized for each system—1 mm for the photothermal pastes and 2 mm for the electrothermal pastes—to ensure reproducible and representative data.

Compression tests. Compression tests were conducted using a DTU-900MH static 100 kN universal testing machine (Daekyung Tech & Tester, Korea). Disk-shaped, cured photothermal samples (3.5 cm in diameter, 5 mm in thickness) were placed on the lower platen of the device, and a compressive load of up to 100 kN was applied by the downward movement of the upper platen at a constant rate of 17 mm/min. During compression, force–displacement curves were recorded, and the macroscopic appearance of the samples was visually inspected after loading.

Cross-cut adhesion test. The surface mechanical robustness of the photothermal composites was evaluated using a cross-cut adhesion test in accordance with the ASTM D3359 standard. Briefly, a series of closely spaced parallel cuts was introduced on the composite surface using a sharp blade, followed by a second set of perpendicular cuts to form a cross-hatched grid pattern. Care was taken to ensure that the incisions penetrated the surface layer to generate localized stress concentrations. Subsequently, a pressure-sensitive adhesive tape was firmly applied over the incised area and rapidly removed. The tested surfaces were then inspected to

examine any signs of material removal, cracking, delamination, or exposure of internal components. No observable detachment of surface material, grid-edge lifting, or crack propagation was detected after tape removal (**Figure S9**). In addition, no leakage or extrusion of liquid metal or PCM was observed from the incised regions, indicating that the functional domains remained securely confined within the bulk composite. These results confirm the strong mechanical integrity of the millimeter-thick composite against severe surface damage involving combined shear and peel stresses.

Differential scanning calorimetry. The latent heat storage and release behaviors of photothermal systems with various compositional ratios were characterized using a DSC25 differential scanning calorimeter (TA Instruments, USA) over a temperature range of -20–50 °C at a scanning rate of 5 °C/min under a nitrogen atmosphere.

Thermal conductivity measurements. The thermal conductivities of both PCM-loaded and PCM-free composites were measured to evaluate the effect of PCM incorporation on the overall heat conduction of the photothermal composites. The transient plane heat source (Hot Disk) method was employed using a TPS 2500 instrument (Hot Disk AB, Sweden) equipped with a Model 5465 F1 sensor. Measurements were carried out in isotropic mode, with the applied power and measurement duration optimized for each specimen to achieve an appropriate probing depth and ensure data reliability. The thermal conductivity of the electrothermal paste containing 30 vol.% filler was also determined using the same method. Each sample was measured three times, and the mean values along with standard deviations are reported.

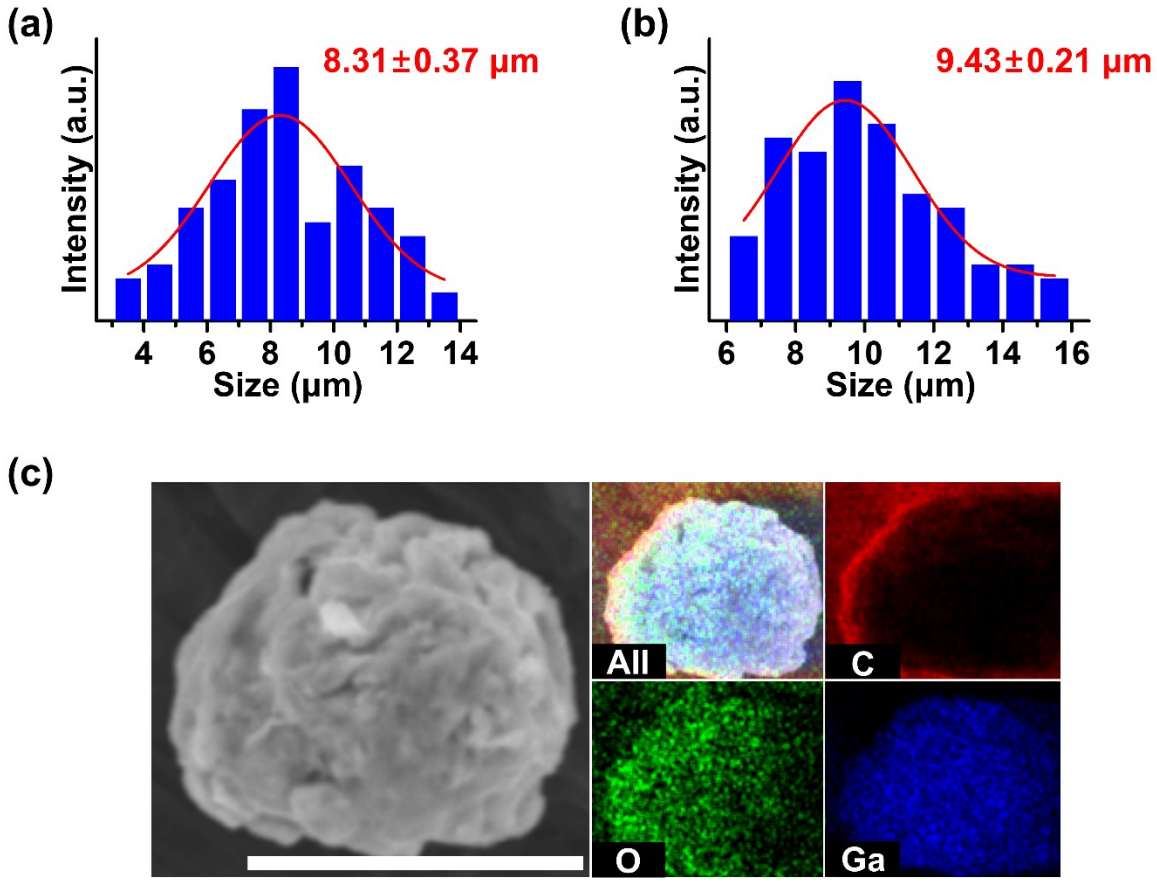

Figure S1. Particle size distributions of the (a) pristine PCM and (b) PCM@Ga microparticles, estimated from optical micrographs. (c) Scanning electron micrograph and energy dispersive spectroscopy elemental mapping of an isolated PCM@Ga particle (scale bar: 10 µm).

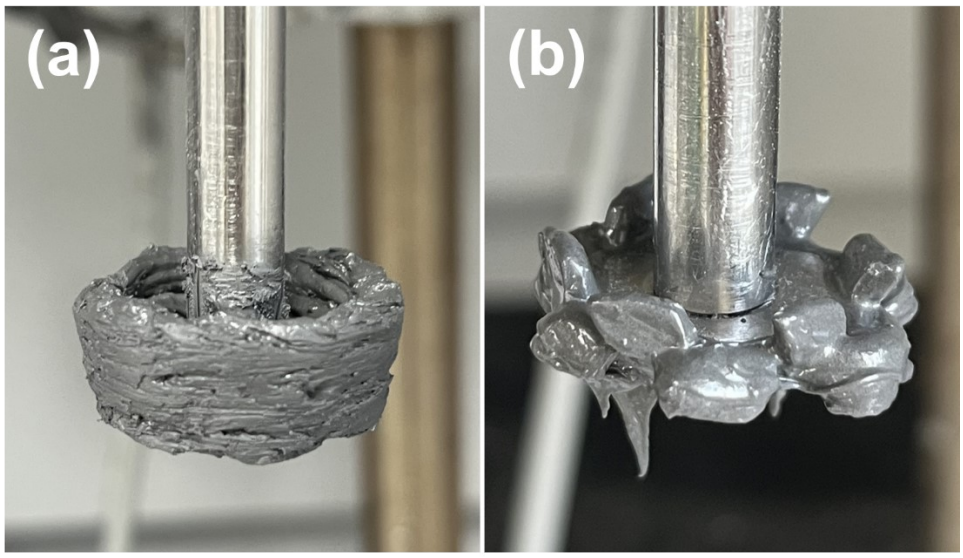

Figure S2. Photographs of the mixing unit after mixing uncured photothermal pastes with (a) $\phi_{PCM@Ga} = 0.1$ and (b) $\phi_{PCM@Ga} = 0.4$.

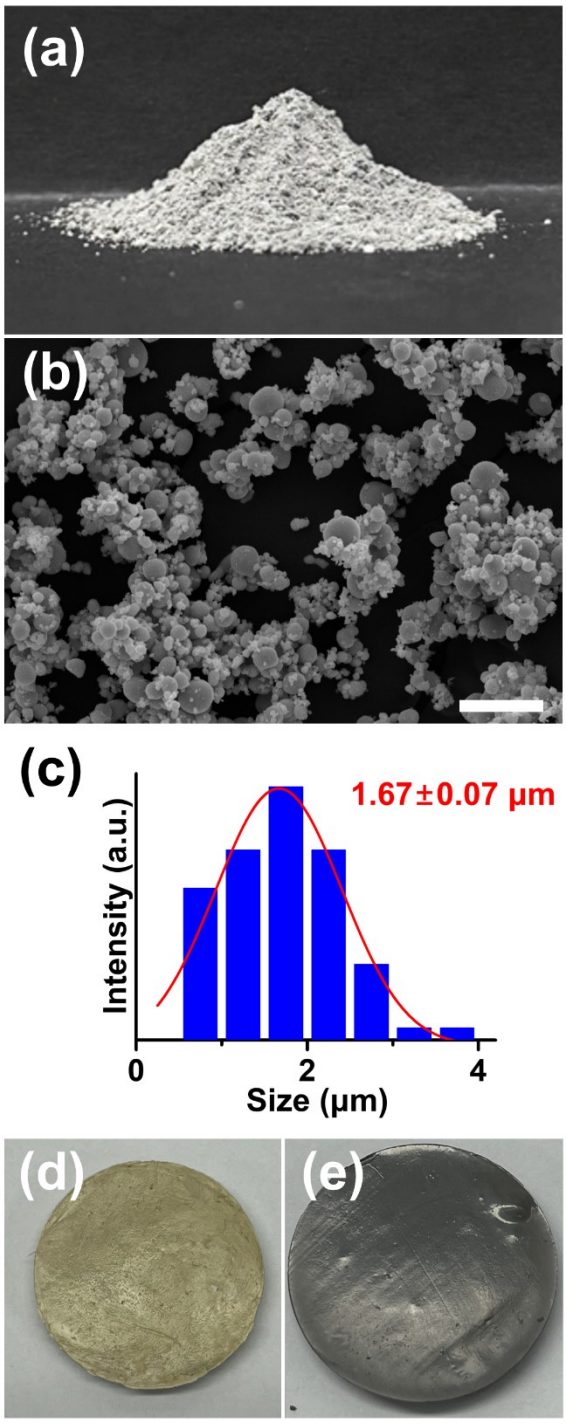

Figure S3. (a) Photograph of micronized Ga powder and (b) corresponding SEM image (scale bar: 10 μm), together with (3) the size distribution. Photographs of the disk-shaped ARE composites (3.5 cm in diameter and 5 mm in thickness: (d) without LM ($\phi_A = 0.5$) and (e) with LM ($\phi_{Ga} = 0.4$ and $\phi_A = 0.1$).

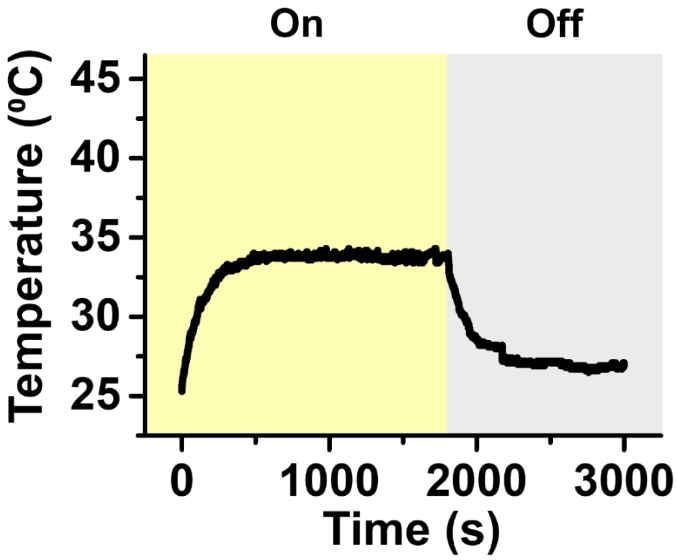

Figure S4. Surface temperature profile of the cured LM-free ARE matrix under simulated solar irradiation (1 SUN) at ambient temperature. The yellow and gray regions indicate the solar-on (30 min) and solar-off (20 min) periods, respectively.

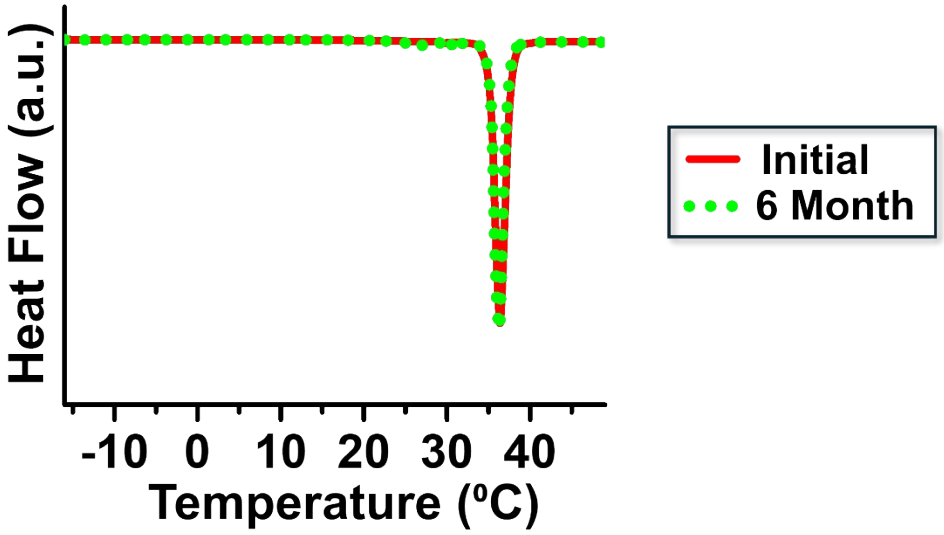

Figure S5. DSC profiles of the cured composite ($\phi_{PCM@Ga}$ = 0.4) during a temperature ramp for the as-prepared sample (solid red) and after six months of storage under ambient conditions (dotted green).

Figure S6. Visual appearance of the cured LM-free ARE matrix after compression.

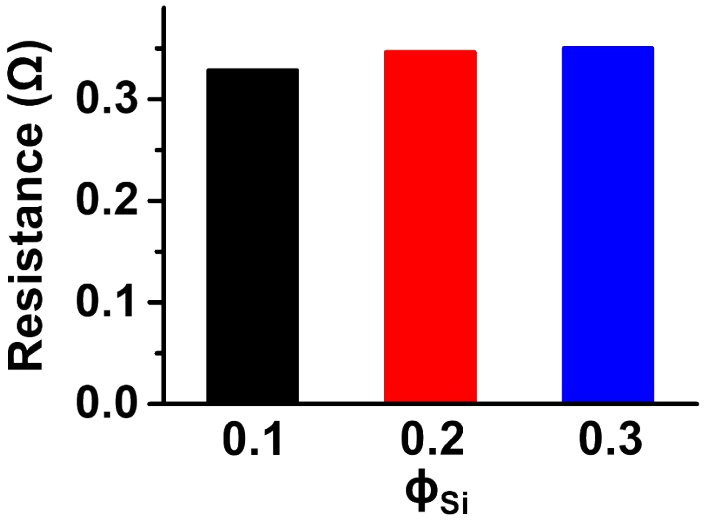

Figure S7. Electrical resistances of single-line patterns (thickness: 0.2 cm, length: 5 cm) fabricated using electrothermal pastes with different Si loadings.

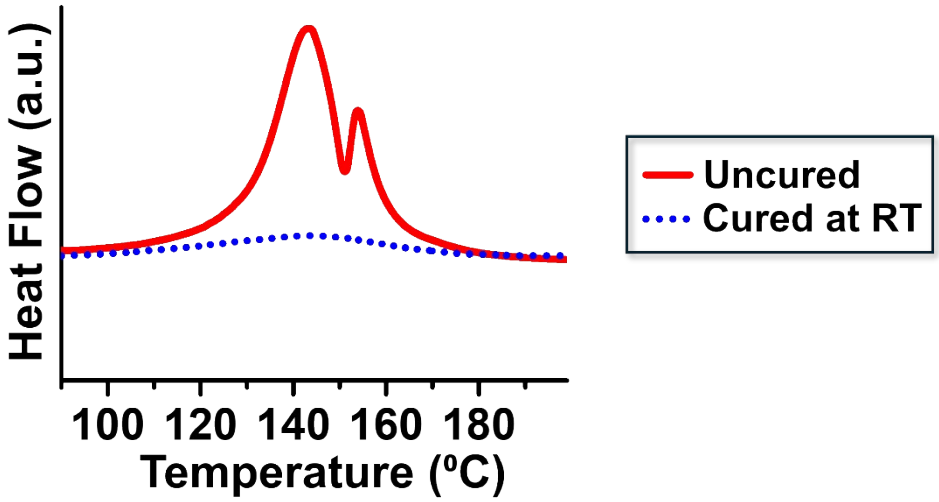

Figure S8. DSC profiles of the uncured ARE matrix ($\phi_F = \phi_A = 0.5$) and the photothermal paste with the optimal formulation ($\phi_F = 0.5$; $\phi_A = 0.2$ and $\phi_{PCM@Ga} = 0.3$). The photothermal paste was naturally cured at room temperature for seven days prior to measurement.

Figure S9. Photograph of the cured photothermal composite layer ($\phi_{PCM@Ga}$ = 0.3, thickness: 5 mm) after performing the cross-cut adhesion test according to ASTM D3359.

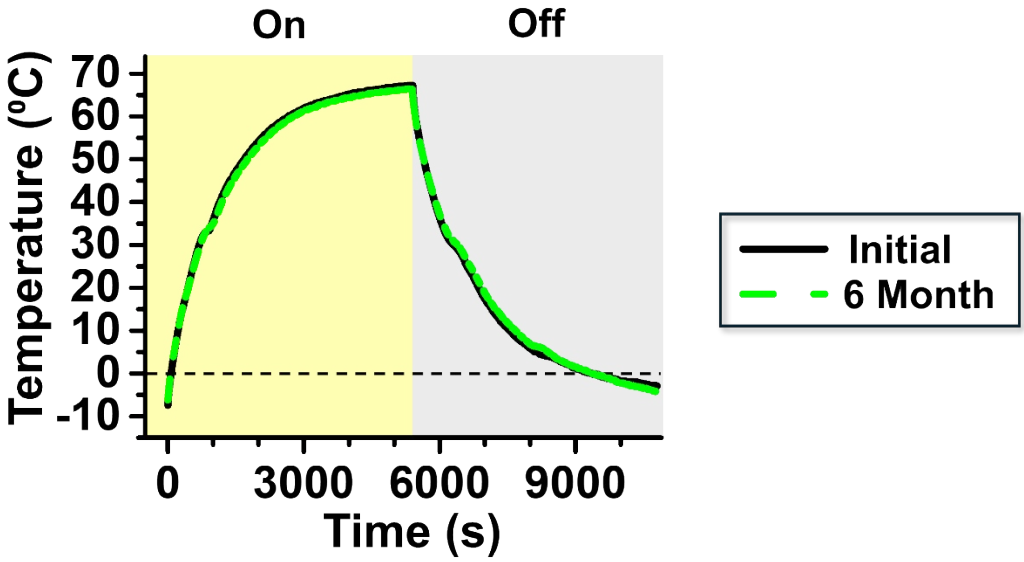

Figure S10. Comparison of representative dual-mode heating profiles between the as-prepared system and that stored under ambient conditions for six months.

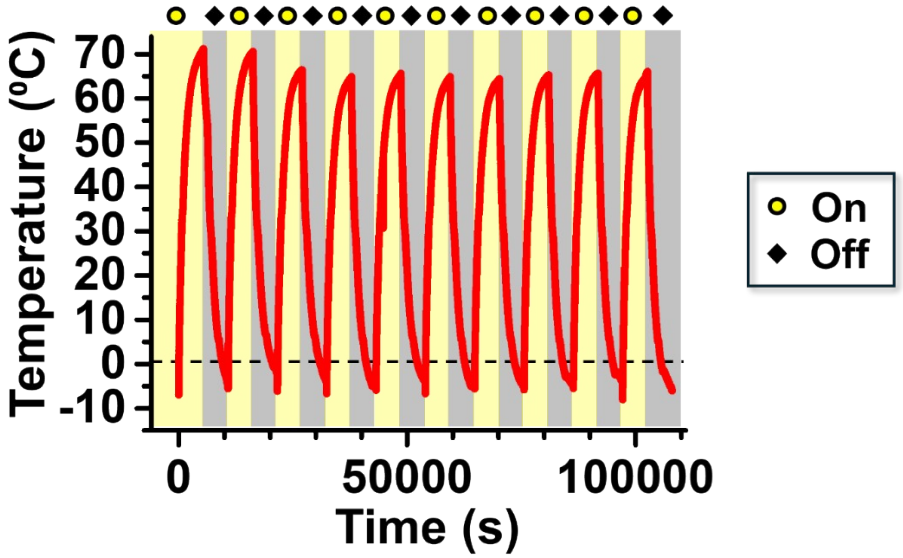

Figure S11. Repeatability of dual-mode heating performance of the integrated system stored under ambient conditions for six months.

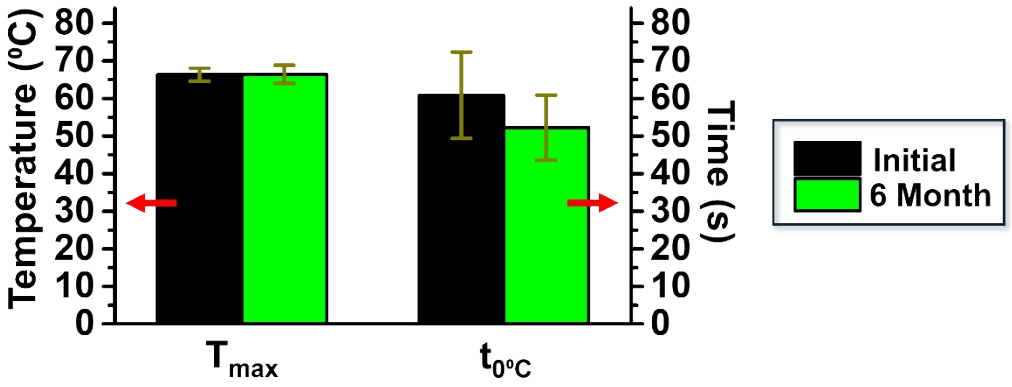

Figure S12. Maximum temperature (T_{max}) and time required to reach the melting point of ice ($t_{0°C}$) for the as-prepared and six-month-aged systems (n: 10).

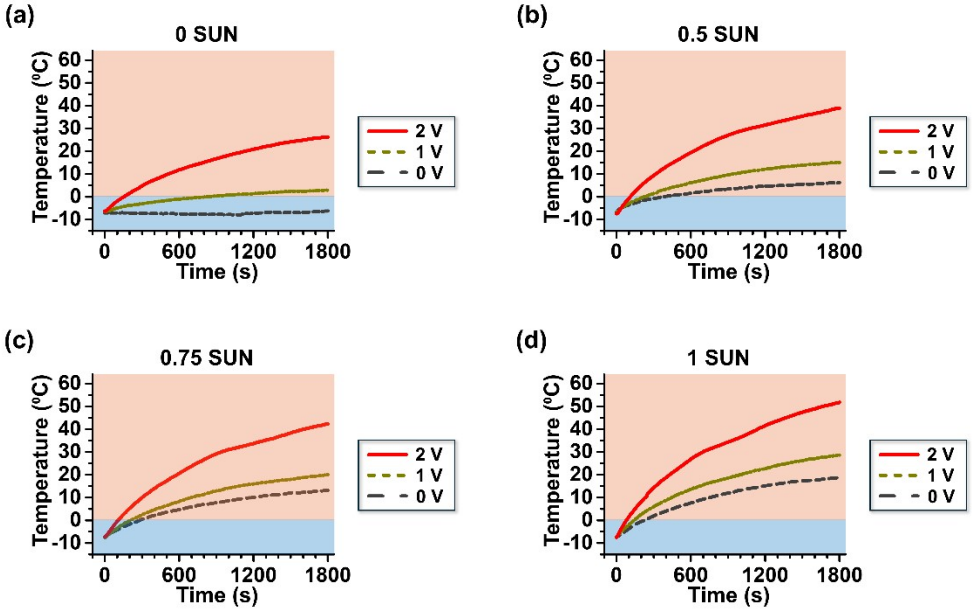

Figure S13. Average temperature profiles within the 4 cm × 4 cm area on the surface of the integrated system under varying solar irradiation levels and electrical inputs: (a) 0 SUN, (b) 0.5 SUN, (c) 0.75 SUN, and (d) 1 SUN.

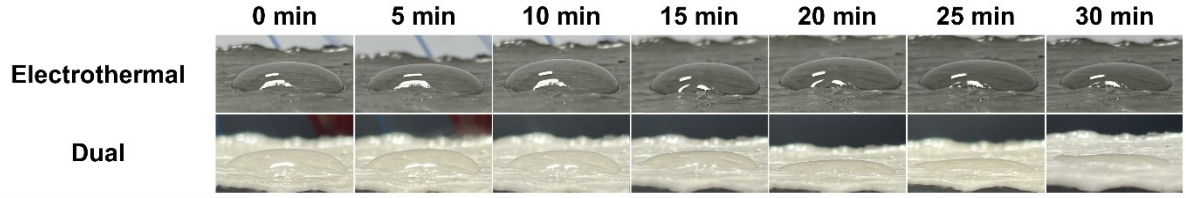

Figure S14. Evaluation of the anti-icing performance of the integrated system under electrothermal (2 V, top) and dual-mode (1 SUN and 2 V, bottom) operation using water droplets (400 μL each). Both experiments were conducted in a subzero environment (−20 °C), where the droplets remained completely unfrozen. Under dual-mode operation, the surface temperature exceeded 50 °C, resulting not only in complete prevention of freezing but also in a gradual reduction in droplet volume due to evaporation.

Photothermal Conversion Efficiency

Following the previous studies (*ACS Nano* **2022**, *16*, 15086–15099; *Small* **2022**, *18*, 2104048; *Chem. Eng. J.* **2024**, *489*, 151338), the photothermal conversion efficiency (η) of the cured ARE composite containing Ga microdroplets was determined at steady state from the balance between absorbed solar input and heat loss to the surroundings:

$$\eta = \frac{h\,S\,(T_{max} - T_{surr})}{q\,A} \tag{1}$$

where h is the heat-transfer coefficient, S is the external surface area participating in heat loss, T_{max} is the steady-state maximum temperature under illumination, T_{surr} is the ambient temperature, q is the solar intensity (0.10 W/cm², 1 SUN), and A is the illuminated area. The h value was obtained from the cooling curve $T(t)$ *vs.* t (where $T(t)$ is the time-dependent specimen temperature and t is time), recorded after switching off the illumination, using a lumped-parameter model. The dimensionless relative temperature $\theta(t)$ is defined as

$$\theta(t) = \frac{T(t) - T_{\text{surr}}}{T_{max} - T_{\text{surr}}} = exp(-\frac{t}{\tau}) \tag{2}$$

and the characteristic time constant τ is given by

$$\tau = \frac{\sum_i m_i c_{p,i}}{h\,S} \tag{3}$$

where m_i and $c_{p,i}$ are the mass and specific heat of component i in the composite. To avoid bias from late-time deviations (e.g., changing effective loss terms at small ΔT), τ was fitted over the early cooling region (first 200 s, corresponding to the fastest decay), yielding an R^2

value of 0.9932. The resulting h from Eq. (3) was then substituted into Eq. (1) to compute η.